Physics Letters B 808 (2020) 135661

Contents lists available at ScienceDirect

Physics Letters B

www.elsevier.com/locate/physletb

Bounds on the non-standard $W^+W^-\gamma$ couplings at the LHeC and the FCC-he

M. Köksal [a], A.A. Billur [b], A. Gutiérrez-Rodríguez [c,d,*], M.A. Hernández-Ruíz [e]

[a] Deparment of Optical Engineering, Sivas Cumhuriyet University, 58140, Sivas, Turkey
[b] Deparment of Physics, Sivas Cumhuriyet University, 58140, Sivas, Turkey
[c] Facultad de Física, Universidad Autónoma de Zacatecas, Apartado Postal C-580, 98060 Zacatecas, Mexico
[d] Unidad Académica de Estudios Nucleares, Mexico
[e] Unidad Académica de Ciencias Químicas, Universidad Autónoma de Zacatecas, Apartado Postal C-585, 98060 Zacatecas, Mexico

ARTICLE INFO

Article history:
Received 12 October 2019
Received in revised form 21 July 2020
Accepted 26 July 2020
Available online 30 July 2020
Editor: G.F. Giudice

Keywords:
Models beyond the standard model
W bosons
Triple gauge boson couplings

ABSTRACT

We examine the potential of the $e^-p \to e^-\gamma^* p \to e^- W^- q' X$ (γ^* is the Weizsacker-Williams photon) reaction to probe the non-standard $W^+W^-\gamma$ couplings at the Large Hadron electron Collider (LHeC) and the Future Circular Collider-hadron electron (FCC-he). Using the effective Lagrangian approach with various values of the center-of-mass energy and integrated luminosity, we find 95% confidence level bounds on the anomalous coupling $\Delta\kappa_\gamma$ and λ_γ parameters. We assume center-of-mass energies of the electron-proton system $\sqrt{s} = 1.30, 1.98, 7.07, 10$ TeV and luminosities $\mathcal{L} = 10 - 1000$ fb^{-1}. The best limits obtained from the process $e^-p \to e^-\gamma^* p \to e^- W^- q' X$ on the anomalous $\Delta\kappa_\gamma$ and λ_γ couplings are $\Delta\kappa_\gamma = |0.00069|$ and $\lambda_\gamma = [-0.0099, 0.0054]$. These bounds show that the process under consideration is a very promising option to probe the non-standard $\Delta\kappa_\gamma$ and λ_γ couplings at the LHeC and the FCC-he. Our results also provide complementary information on other results for $\Delta\kappa_\gamma$ and λ_γ couplings.

1. Introduction

The Standard Model (SM) of Elementary Particle Physics [1–3] is extremely predictive and has been tested in numerous aspects with impressive precision. The SM is a very powerful tool to predict the characteristics, the behavior and the interactions of the elementary particles. Therefore, it is very important to measure particle properties and interactions in the most accurate way possible to better understand the SM, to refine it and to test its global consistency. The anomalous Triple-Gauge-Boson Couplings (aTGC) and anomalous Quartic Gauge Boson Couplings (aQGC) of the $W^\pm$ bosons: $W^+W^-\gamma$, W^+W^-Z, $WZ\gamma$, $W\gamma\gamma$, $W^+W^-\gamma\gamma$, $W^+W^-Z\gamma$, W^+W^-ZZ and $W^+W^-W^+W^-$ are key elements in the search for the new physics beyond the SM (BSM) since any discrepancy in the measured value with respect to the predicted value could reveal new phenomena other than the SM.

The anomalous contribution to the $W^+W^-\gamma$ vertex, i.e., $\Delta\kappa_\gamma$ and λ_γ parameters, has been studied for the ATLAS [4], CMS [5], CDF [6], D0 [7], ALEP, DELPHI, L3, OPAL [8] and TESLA [9] experiments. With respect to the anomalous $\Delta\kappa_\gamma$ and λ_γ couplings, our bounds compared favorably with those reported by the ATLAS, CMS, CDF, D0, ALEP, DELPHI, L3, OPAL and TESLA [9] Collaborations (see Table 1), respectively. Furthermore, our bounds on $\Delta\kappa_\gamma$ and λ_γ are competitive with the phenomenological limits which are obtained assuming the parameters of the Large Hadron Collider (LHC) [10], the Large Hadron electron Collider (LHeC) [11], the International Linear Collider (ILC) [13], the Circular Electron Positron Collider (CEPC) [12] and the Compact Linear Collider (CLIC) [14]. Our bounds on the aTGC are discussed in Subsection 3.2. For other experimental and phenomenological reports on $\Delta\kappa_\gamma$ and λ_γ, see Table 1 as well as Refs. [15–32].

A new possibility anticipated for future e^-p colliders is to operate this machine as γe and γp collisions. This can be done by converting incoming electrons or protons into an intense beam of high-energy photons. e^-p colliders can also provide the opportunity to examine $\gamma^* e$ and $\gamma^* p$ modes with quasi-real photons.

In this work, we have investigated the process $e^-p \to e^-\gamma^* p \to e^- W^- q' X$ through the subprocess $\gamma^* p \to W^- q'$ at e^-p colliders. Here, γ^* photons in the initial state are obtained by the Equivalent Photon Approximation (EPA) [33–35]. The EPA assumes that quasi-real photons emitted from the electrons have a low virtuality

* Corresponding author.
E-mail addresses: mkoksal@cumhuriyet.edu.tr (M. Köksal), abillur@cumhuriyet.edu.tr (A.A. Billur), alexgu@fisica.uaz.edu.mx (A. Gutiérrez-Rodríguez), mahernan@uaz.edu.mx (M.A. Hernández-Ruíz).

https://doi.org/10.1016/j.physletb.2020.135661

Table 1
Summary of experimental and phenomenological bounds at 95% C.L. on the aTGC $\Delta\kappa_\gamma$ and λ_γ from the present and future colliders.

Model	$\Delta\kappa_\gamma$	λ_γ	C. L.	Reference
SM	0	0		[1–3]
Experimental limit	$\Delta\kappa_\gamma$	λ_γ	C. L.	Reference
ATLAS Collaboration	[-0.061, 0.064]	[-0.013, 0.013]	95%	[4]
CMS Collaboration	[-0.044, 0.063]	[-0.011, 0.011]	95%	[5]
CDF Collaboration	[-0.158, 0.255]	[-0.034, 0.042]	95%	[6]
D0 Collaboration	[-0.158, 0.255]	[-0.034, 0.042]	95%	[7]
ALEP, DELPHI, L3, OPAL	[-0.099, 0.066]	[-0.059, 0.017]	95%	[8]
Phenomenological limit	$\Delta\kappa_\gamma$	λ_γ	C. L.	Reference
LHC	[-0.182, 0.793]	[-0.065, 0.065]	95%	[10]
LHeC	[[-0.0016, 0.0024]	[-0.0040, 0.0043]	95%	[11]
CEPC	[-0.00045, 0.00045]	[-0.00033, 0.00033]	95%	[12]
ILC	[-0.00037, 0.00037]	[-0.00051, 0.00051]	95%	[13]
CLIC	[-0.00007, 0.00007]	[-0.00004, 0.00004]	95%	[14]

and scatter with small angles from the beam pipe. Their virtuality is very low and it is a good approximation to assume that they are on the mass shell. Therefore, when an electron emits a quasi-real photon, it should also be scattered with a small angle and scattered intact electrons should exit the central detector without being detected. For a $\gamma^* p$ collision, one of the forward regions of the central detector has a significant lack of energy. The region which is lacking particles defines a forward large rapidity gap. Usual $e^- p$ deep inelastic processes can be rejected by applying a selection cut on this quantity. Another experimental signature is provided by the forward detectors. When an intact electron is scattered with a large pseudorapidity, it escapes detection from the central detectors. However, since its energy is lower than the beam energy, its trajectory decouples from the beam path into the very forward region. Forward detectors can detect particles with a large pseudorapidity, and the detection of scattered electrons and protons by the forward detectors provides a characteristic signature. The detection of the photon induced reactions involves a missing energy signature production in addition to the above signatures. Finally, the operation of forward detectors in conjunction with central detectors with precise timing can efficiently reduce backgrounds. LHeC Collaboration has a program of forward physics with extra detectors located in a region between a few tens up to several hundreds of meters from the interaction point [36,37].

The measurement of the $W^+W^-\gamma$ vertex at the future LHeC at CERN is discussed through the process $e^- p \to e^- \mu \nu_\mu j$ in Ref. [11]. Although the $e^- p \to e^- \mu \nu_\mu j$ process is very similar to the $e^- p \to e^- \gamma^* p \to e^- W^- q' X$ process examined in this study, there are significant differences between the two. Since the photons contained in this process can have high virtuality, scattered electrons are detected by central detectors as seen in equation 4 on page 4 of their study. We understand that the basic cut on leptons in the final state is $\Delta R_{\ell\ell} > 0.4$.

As explained above, the two studies are quite different. While two leptons (an electron and a muon) in the final state in Ref. [11] are detected by central detectors, only one electron in the final state is detected in our study. The photon emitted by the electron is detected by forward detectors because the virtuality of the photons emitted from the electrons is very low. While the virtuality of photons is small, they are considered to be quasi-real. In the process considered in Ref. [11], the photons emitted are not real.

These studies underline the importance of measuring the anomalous $\Delta\kappa_\gamma$ and λ_γ gauge couplings in several different channels, contexts and colliders. For instance, measurements can be made in hadron-hadron, lepton-lepton and hadron-lepton colliders, such as the LHC, the CLIC and the Future Circular Collider (FCC) at CERN. Furthermore, these colliders will be very useful operating in the $e^-\gamma$, $\gamma\gamma$, $e^-\gamma^*$, $\gamma^* p$ and $\gamma^*\gamma^*$ modes. One characteristic that distinguishes the FCC from the linear colliders is that the FCC studies and explores the feasibility of different particle collider scenarios in order to significantly increase the energy and luminosity as compared to existing colliders. It aims to complement existing technical designs for linear colliders.

With these arguments, we determine the production cross-section as well as model-independent bounds for the non-standard $W^+W^-\gamma$ couplings at the LHeC and the Future Circular Collider-hadron electron (FCC-he) [36–41] through the $e^- p \to e^- \gamma^* p \to e^- W^- q' X$ reaction, where γ^* is the quasi-real photon in the Weizsacker-Williams Approximation (WWA) and X represents the proton remnants after deep inelastic scattering. We use projections for runs at center-of-mass energies of 1.30, 1.98, 7.07 TeV and 10 TeV and total integrated luminosities of 10, 30, 50, 70, 100, 300, 500, 700 and 1000 fb^{-1}, respectively. In addition, to characterize possible deviations from the SM predictions on the anomalous $\Delta\kappa_\gamma$ and λ_γ couplings, we employ the effective Lagrange technique where the SM is extended by a set of dimension-six operators.

The rest of this paper is organized as follows: In Sect. 2, a brief review of the operators in effective Lagrangian is provided. In Sect. 3, we compute the total cross-section and derive bounds for the anomalous $\Delta\kappa_\gamma$ and λ_γ couplings at the LHeC and the FCC-he. In Sect. 4, we present our conclusions.

2. A brief review of the non-standard $W^+W^-\gamma$ couplings

Deviations from the SM prediction are usually parameterized by an effective Lagrangian which contains a series of higher-dimensional effective operators suppressed by the scale of new physics Λ in addition to the renormalizable part of the SM.

For the analysis of anomalous $W^+W^-\gamma$ couplings, we use the Hagiwara, Ishihara, Szalapski and Zeppenfeld (HISZ) basis first introduced by Hagiwara et al. in Ref. [42] for our effective Lagrangian. A useful discussion for the choice of basis and alternative choices is given in [43].

In order to analyze the bounds on the non-standard $W^+W^-\gamma$ couplings $\Delta\kappa_\gamma$ and λ_γ through the process $e^- p \to e^- \gamma^* p \to e^- W^- q' X$, we adopt the effective Lagrangian:

$$\mathcal{L}_{eff} = \mathcal{L}^{(4)}_{SM} + \sum_i \frac{C_i^{(6)}}{\Lambda^2} \mathcal{O}_i^{(6)} + \text{h.c.}, \tag{1}$$

where $\mathcal{L}^{(4)}_{SM}$ denotes the renormalizable SM Lagrangian and the non-SM part contains the $\mathcal{O}_i^{(6)}$ gauge-invariant operators of mass dimension-six. The index i runs over all operators of the given

mass dimension. The mass scale is set by Λ, and the coefficients C_i are the dimensionless parameters determined once the full theory is known.

The effective Lagrangian relevant to the analysis of aTGC reads:

$$\mathcal{L}_{eff} = \frac{1}{\Lambda^2}\Big[C_W\mathcal{O}_W + C_B\mathcal{O}_B + C_{WWW}\mathcal{O}_{WWW} + C_{\tilde{W}WW}\mathcal{O}_{\tilde{W}WW} + C_{\tilde{W}}\mathcal{O}_{\tilde{W}} + \text{h.c.}\Big]. \quad (2)$$

Three of them are the independent C and P conserving operators:

$$\mathcal{O}_W = \big(D_\mu\Phi\big)^\dagger \hat{W}^{\mu\nu}\big(D_\nu\Phi\big), \quad (3)$$

$$\mathcal{O}_B = \big(D_\mu\Phi\big)^\dagger \hat{B}^{\mu\nu}\big(D_\nu\Phi\big), \quad (4)$$

$$\mathcal{O}_{WWW} = Tr\big[\hat{W}_{\mu\nu}\hat{W}^{\nu\rho}\hat{W}^{\mu}_{\rho}\big]. \quad (5)$$

D_μ is the covariant derivative, Φ is the Higgs doublet field and $\hat{B}_{\mu\nu}$, and $\hat{W}_{\mu\nu}$ are the $U(1)_Y$ and $SU(2)_L$ gauge field strength tensors. The coefficients of the operators C_W/Λ^2, C_B/Λ^2 and C_{WWW}/Λ^2 are zero in the SM.

If we allow for C and/or P violation, the two remaining operators are:

$$\mathcal{O}_{\tilde{W}WW} = Tr\big[\hat{\tilde{W}}_{\mu\nu}\hat{W}^{\nu\rho}\hat{W}^{\mu}_{\rho}\big], \quad (6)$$

$$\mathcal{O}_{\tilde{W}} = \big(D_\mu\Phi\big)^\dagger \hat{\tilde{W}}^{\mu\nu}\big(D_\nu\Phi\big). \quad (7)$$

There are therefore three C and P conserving dimension-six operators and two operators that violate C and/or P.

Based on this methodology, the effective Lagrangian to describe the $W^+W^-\gamma$ coupling can be parameterized as [17,44]:

$$\begin{aligned}\mathcal{L}_{WW\gamma} = &-ig_{WW\gamma}\Big[g_1^\gamma(W^\dagger_{\mu\nu}W^\mu A^\nu - W^{\mu\nu}W^\dagger_\mu A_\nu) \\ &+ \kappa_\gamma W^\dagger_\mu W_\nu A^{\mu\nu} + \frac{\lambda_\gamma}{M_W^2}W^\dagger_{\rho\mu}W^\mu_\nu A^{\nu\rho}\Big] \\ &+ ig_4^\gamma W^+_\mu W^-_\nu(\partial^\mu V^\nu + \partial^\nu V^\mu) \\ &- ig_5^\gamma\epsilon^{\mu\nu\rho\sigma}(W^+_\mu\partial_\rho W^-_\nu - \partial_\rho W^+_\mu W^-_\nu)V_\sigma \\ &+ \tilde{\kappa}_\gamma W^+_\mu W^-_\nu\tilde{V}^{\mu\nu} + \frac{\tilde{\lambda}_\gamma}{m_W^2}W^{+\nu}_\mu W^{-\rho}_\nu\tilde{V}^\mu_\rho, \end{aligned} \quad (8)$$

where $g_{WW\gamma} = e$, $V_{\mu\nu} = \partial_\mu V_\nu - \partial_\nu V_\mu$ with $V_\mu = W_\mu, A_\mu$. The first three terms of the above equation respect C and P, and the remaining four terms violate C and/or P. Electromagnetic gauge invariance implies that $g_1^\gamma = 1$ and $g_4^\gamma = g_5^\gamma = 0$. There are thus two independent C and P conserving parameters: κ_γ and λ_γ; two C and/or P violating parameters: $\tilde{\kappa}_\gamma$ and $\tilde{\lambda}_\gamma$.

In this study, we focus on the g_1^γ, κ_γ and λ_γ parameters that are CP-conserving. In the SM, their values are $g_1^\gamma = \kappa_\gamma = 1$ and $\lambda_\gamma = 0$ at the tree level.

The three dimension-six operators given by Eq. (2) are related to the $W^+W^-\gamma$ aTGC via [18,42,45]:

$$\kappa_\gamma = 1 + \Delta\kappa_\gamma, \quad (9)$$

with

$$\Delta\kappa_\gamma = \frac{m_W^2}{2\Lambda^2}(C_W + C_B), \quad (10)$$

$$\lambda_\gamma = \frac{3g^2m_W^2}{2\Lambda^2}C_{WWW}. \quad (11)$$

From the effective Lagrangian given in Eq. (8), the Feynman rule for the anomalous $W^+W^-\gamma$ vertex function that is the most generally CP-conserving and consistent with gauge and Lorentz invariance of the SM is given by [17]:

$$\begin{aligned}\Gamma^{WW\gamma}_{\mu\nu\rho} = &\,e\Big[g_{\mu\nu}(p_1-p_2)_\rho + g_{\nu\rho}(p_2-p_3)_\mu + g_{\rho\mu}(p_3-p_1)_\nu \\ &+ \Delta\kappa_\gamma\Big(g_{\rho\mu}p_{3\nu} - g_{\nu\rho}p_{3\mu}\Big) \\ &+ \frac{\lambda_\gamma}{M_W^2}\Big(p_{1\rho}p_{2\mu}p_{3\nu} - p_{1\nu}p_{2\rho}p_{3\mu} \\ &- g_{\mu\nu}(p_2\cdot p_3 p_{1\rho} - p_3\cdot p_1 p_{2\rho}) \\ &- g_{\nu\rho}(p_3\cdot p_1 p_{2\mu} - p_1\cdot p_2 p_{3\mu}) \\ &- g_{\mu\rho}(p_1\cdot p_2 p_{3\nu} - p_2\cdot p_3 p_{1\nu})\Big)\Big], \end{aligned} \quad (12)$$

where p_1 represents the momentum of the photon and p_2 and p_3 symbolize the momenta of $W^\pm$ bosons. The first three terms in Eq. (12) correspond to the SM couplings, while the terms with $\Delta\kappa_\gamma$ and λ_γ give rise to the anomalous triple gauge boson couplings.

As shown in Table 1, several searches on these anomalous $\Delta\kappa_\gamma$ and λ_γ couplings of $W^+W^-\gamma$ vertex were performed by the LEP, Tevatron and LHC experiments.

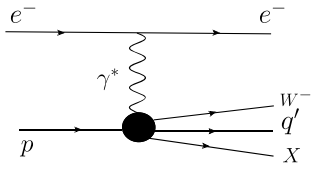

Fig. 1. A schematic diagram for the process $e^-p \to e^-\gamma^*p \to e^-W^-q'X$.

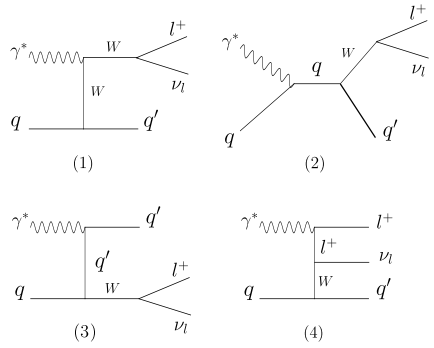

Fig. 2. Feynman diagrams contributing to the sub-process $\gamma^*q \to W^-q'$.

3. Cross-section of the process $e^-p \to e^-\gamma^*p \to e^-W^-q'X$ and bounds on the anomalous $\Delta\kappa_\gamma$ and λ_γ couplings at the LHeC and the FCC-he

3.1. Cross-section of the process $e^-p \to e^-\gamma^*p \to e^-W^-q'X$ at the LHeC and the FCC-he

At the LHeC and the FCC-he, the aTGC can be directly probed via single-$W^\pm$ production. We therefore focus on the process $e^-p \to e^-\gamma^*p \to e^-W^-q'X$ as well as its corresponding subprocesses (see Figs. 1 and 2):

$$\gamma^*u \to W^+d \to l^+\nu_l d, \quad (13)$$

$$\gamma^*u \to W^+s \to l^+\nu_l s, \quad (14)$$

$$\gamma^*c \to W^+s \to l^+\nu_l s, \quad (15)$$

$$\gamma^*c \to W^+d \to l^+\nu_l d, \quad (16)$$

Table 2
The total cross-sections of Signal (S) and Background (B_{SM}) for the three kinematic cuts used in the analysis of the process $e^-p \to e^-\gamma^* p \to e^- W^- q' X$ for $\sqrt{s} =$ 1.30, 1.98, 7.07, 10 TeV at the LHeC and the FCC-he.

$\sigma(e^-p \to e^-\gamma^* p \to e^- W^- q' X)$ (pb)						
LHeC	$\sqrt{s} = 1.30$ TeV			$\sqrt{s} = 1.98$ TeV		
Cuts	$S+B_{SM}$ ($\lambda_\gamma = 0.3$)	$S+B_{SM}$ ($\Delta\kappa_\gamma = 1$)	B_{SM}	$S+B_{SM}$ ($\lambda_\gamma = 0.3$)	$S+B_{SM}$ ($\Delta\kappa_\gamma = 1$)	B_{SM}
cuts 1	1.848	2.910	1.772	3.717	5.929	3.445
cuts 2	0.958	1.853	0.883	2.121	4.003	1.853
cuts 3	0.683	1.375	0.612	1.559	3.013	1.319
FCC-he	$\sqrt{s} = 7.07$ TeV			$\sqrt{s} = 10$ TeV		
Cuts	$S+B_{SM}$ ($\lambda_\gamma = 0.3$)	$S+B_{SM}$ ($\Delta\kappa_\gamma = 1$)	B_{SM}	$S+B_{SM}$ ($\lambda_\gamma = 0.3$)	$S+B_{SM}$ ($\Delta\kappa_\gamma = 1$)	B_{SM}
cuts 1	18.834	25.884	13.975	32.110	39.909	20.858
cuts 2	13.199	19.260	8.507	24.497	30.523	13.291
cuts 3	10.481	14.850	6.210	20.180	23.773	9.837

$$\gamma^*\bar{d} \to W^+\bar{u} \to l^+\nu_l\bar{u}, \tag{17}$$
$$\gamma^*\bar{d} \to W^+\bar{c} \to l^+\nu_l\bar{c}, \tag{18}$$
$$\gamma^*\bar{s} \to W^+\bar{c} \to l^+\nu_l\bar{c}, \tag{19}$$
$$\gamma^*\bar{s} \to W^+\bar{u} \to l^+\nu_l\bar{u}, \tag{20}$$
$$\gamma^*\bar{b} \to W^+\bar{t} \to l^+\nu_l\bar{t}, \tag{21}$$

where $l^+ = e^+, \mu^+$; $\nu_l = \nu_e, \nu_\mu$ and γ^* is the quasi-real photon in the WWA. It is worth noting that in Eqs. (13)–(21), we take into account interactions between different flavors of the quarks due to off-diagonal elements of the Cabibbo-Kobayashi-Maskawa matrix.

In this type of $\gamma^* p$ interactions, the emitted quasi-real photon γ^* is scattered with small angles from the beam pipe of e^- [33,46–50]. As these photons have low virtuality, they are almost on the mass shell. These processes can be described by the EPA [33–35] using the WWA. The EPA has many advantages such as reaching crude numerical predictions via simple formulae. Furthermore, it may principally ease the experimental analysis because it enables directly achieving a rough cross-section for the $\gamma^* p \to X$ process via the examination of the main process $e^- p \to e^- X p$ where X represents objects produced in the final state. The production of high mass objects is particularly interesting at the $e^- p$ colliders, and the rate of this production is limited by the photon luminosity at high invariant mass while the $\gamma^* p$ process at the $e^- p$ colliders arises from quasi-real photon emitted from the incoming beams. Moreover, using the EPA, new physics searches BSM have been theoretically and experimentally examined at the LEP, the Tevatron and the LHC [51–71].

In the EPA, the energy spectrum of the photons emitted from electron beams is given by the following analytical formula [33, 72]:

$$f_{\gamma_e^*}(x_1) = \frac{\alpha}{\pi E_e}\Big\{[\frac{1-x_1+x_1^2/2}{x_1}]log(\frac{Q^2_{max}}{Q^2_{min}}) - \frac{m_e^2 x_1}{Q^2_{min}}(1-\frac{Q^2_{min}}{Q^2_{max}}) - \frac{1}{x_1}[1-\frac{x_1}{2}]^2 log\Big(\frac{x_1^2E_e^2+Q^2_{max}}{x_1^2E_e^2+Q^2_{min}}\Big)\Big\}, \tag{22}$$

where $x_1 = E_{\gamma_e^*}/E_e$ is the energy fraction transferred from the electron to the photon and $Q^2_{\max} = 2$ GeV^2 is maximum virtuality of the photon. The minimum value of the $Q^2_{\min}$ is given by:

$$Q^2_{\min} = \frac{m_e^2 x_1^2}{1-x_1}. \tag{23}$$

Therefore, the total cross-section of the $e^- p \to e^-\gamma^* p \to e^- W^- q' X$ reaction is determined by:

$$\sigma(e^-p \to e^-\gamma^* p \to e^- W^- q' X) = \int f_{\gamma_e^*}(x_1)\hat{\sigma}(\gamma^* q \to W^- q')dx_1. \tag{24}$$

To numerically evaluate the total cross-section, we use CTEQ6L1 [73] for the parton distribution functions and the $W^+W^-\gamma$ vertex is embedded in CalcHEP package [72] together with the energy spectrum of the photon. For all calculations in this paper, we assume that the center-of-mass energies of the electron-proton system are 1.30, 1.98, 7.07 and 10 TeV, respectively. In addition, we apply basic cuts to reduce the background and optimize the signal. The cuts we have chosen are the default values in $e^- p$ colliders [11,21,36]. To apply realistic cut values, there is no experimental process that uses our process to investigate the anomalous $W^+W^-\gamma$ couplings in $e^- p$ colliders. However, there are two studies related to the anomalous $W^+W^-\gamma$ couplings in $e^- p$ colliders. In the first study Ref. [11], the following cuts were used:

$$p_{T_j} > 20 \text{ GeV}, \quad p_{T_\ell} > 10 \text{ GeV}, \tag{25}$$
$$|\eta_j| < 5, \quad |\eta_\ell| < 5. \tag{26}$$

One noticeable situation here is that they do not apply any cuts on the missing energy in calculations.

In the second study [21], we can assume the cuts are given by:

$$p_{T_j} > 20 \text{ GeV}, \quad p_{T_\nu} > 20 \text{ GeV}, \quad p_{T_\gamma} > 50 \text{ GeV}, \tag{27}$$
$$|\eta_j| < 3.5, \quad |\eta_\ell| < 3.5. \tag{28}$$

As seen from the above studies, the applied cuts for particles in the final states of the examined processes are different from each other, and we benefited from these cuts to reduce the backgrounds and optimize the signal in our study.

We also obtained a simple cutflow of both signal and background for four different values of the center-of-mass, making a grouping for the cuts [11,21] as follows:

$$\text{Cuts} \quad 1: |\eta_j| < 5, \quad |\eta_\ell| < 2.5, \tag{29}$$
$$\text{Cuts} \quad 2: p_{T_j} > 20 \text{ GeV}, \tag{30}$$
$$\text{Cuts} \quad 3: p_{T_\nu} > 20 \text{ GeV}, \quad p_{T_\ell} > 20 \text{ GeV}. \tag{31}$$

We show the total cross-sections of Signal (S) and Background (B_{SM}) for the kinematic cuts given by Eqs. (29)–(31) for the analysis of the process $e^- p \to e^-\gamma^* p \to e^- W^- q' X$ for 1.30, 1.98, 7.07 and 10 TeV in Table 2. We consider parton-level simulations in our calculations.

Table 2 also shows that the S/B_{SM} ratio increases after each applied cut and the total cross-section of the S plus B_{SM} with $\Delta\kappa_\gamma = 1$ is larger when the kinematic cuts given by Eqs. (29)–(31) are applied. We therefore get better limitations for $\Delta\kappa_\gamma$ than for λ_γ.

In Figs. 3 and 4, we plot the total cross sections of the $e^- p \to e^-\gamma^* p \to e^- W^- q' X$ process. These graphs describe the behavior

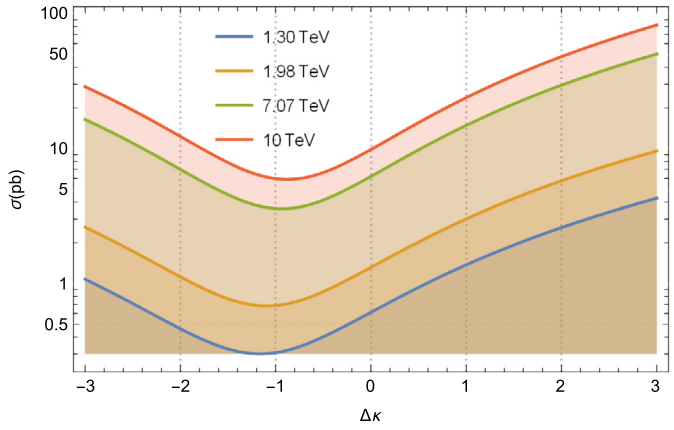

Fig. 3. The total cross-sections of the process $e^-p \to e^-\gamma^* p \to \nu_e W^- p$ as a function of $\Delta\kappa_\gamma$ for center-of-mass energies of $\sqrt{s} = 1.30, 1.98, 7.07, 10$ TeV at the LHeC and the FCC-he.

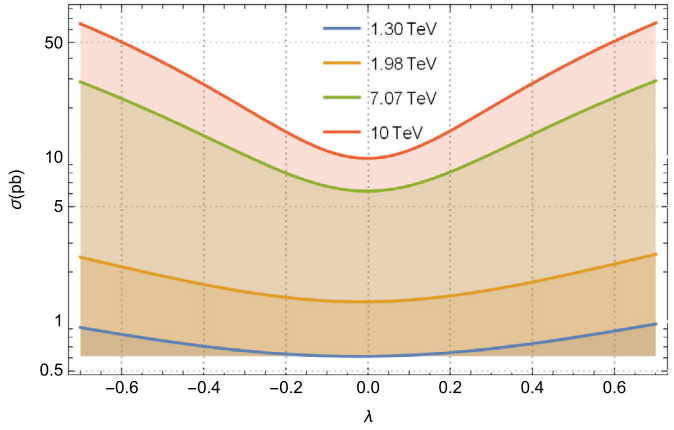

Fig. 4. Same as in Fig. 3, but for λ_γ.

of the total cross-section $\sigma(\Delta\kappa_\gamma, \lambda_\gamma, \sqrt{s})$ in the context of effective Lagrangians and as a function of the anomalous parameters $\Delta\kappa_\gamma/\lambda_\gamma$, maintaining the fixed center-of-mass energy of the collider assumed for values $\sqrt{s} = 1.30, 1.98, 7.07$ and 10 TeV. The total cross-section $\sigma(\Delta\kappa_\gamma, \lambda_\gamma, \sqrt{s})$ increases to a value of the order of $\sim$ 90 pb (70 pb) on a scale of center-of-mass energies of 1.30 up to 10 TeV. We conclude from this analysis that the total cross-section of single W-boson production depends significantly on the center-of-mass energy of the collider as well as on the anomalous parameters $\Delta\kappa_\gamma$ and λ_γ. This means that the effective area of the collision increases for very high energy ranges. The aTGC and the parameters of the colliders both tend to increase the cross-section of the single production W-boson. However, as seen in Fig. 3, the effect of interference can lower the cross-section for negative values of $\Delta\kappa_\gamma$.

3.2. Bounds on the non-standard $\Delta\kappa_\gamma$ and λ_γ couplings at the LHeC and the FCC-he

A model-independent fit procedure to determine the precision of a quantity is based on the construction of a χ^2 function from all observables. The χ^2 function to obtain our bounds on the non-standard $\Delta\kappa_\gamma$ and λ_γ couplings at the 95% Confidence Level (C.L.) can thus be expressed as [15,74–78]:

$$\chi^2(\Delta\kappa_\gamma, \lambda_\gamma) = \left(\frac{\sigma_{SM} - \sigma_{NP}(\sqrt{s}, \Delta\kappa_\gamma, \lambda_\gamma)}{\sigma_{SM}\sqrt{(\delta_{st})^2 + (\delta_{sys})^2}} \right)^2 . \tag{32}$$

σ_{SM} is the SM cross-section and $\sigma_{NP}(\sqrt{s}, \Delta\kappa_\gamma, \lambda_\gamma)$ is the cross-section containing both the non-standard and SM contributions. $\delta_{st} = \frac{1}{\sqrt{N_{SM}}}$ is the statistical error and δ_{sys} is the systematic error. The number of events is given by $N_{SM} = \mathcal{L}_{int} \times \sigma_{SM}$.

The systematic uncertainties play a key role in the measurement of physical quantities such as the anomalous $\Delta\kappa_\gamma$ and λ_γ couplings. Systematic uncertainties arise from the nature of the measurement apparatus, from assumptions made by the experimenter or from the model used to make inferences based on the observed data. In this sense, an important aspect of our study is the incorporation of systematic uncertainies when identifying the W-boson. Some of the most common sources of systematic uncertainties are: Background, Luminosity and PDF (Parton Distribution Functions). In our study, we considered the impact of a few representative values of a total systematic uncertainties.

We made our calculations taking into account the basic acceptance cuts given by Eqs. (29)–(31) for the LHeC and the FCC-he to reduce the background and optimize the sensitivity of the signal. In addition, we consider the systematic uncertainties given by the representative values $\delta_{sys} = 0\%, 1\%, 5\%, 10\%$ [79,80].

We may assume that the LHeC and the FCC-he will be built in the coming years which will substantially improve the precision achieved in the Hadron Electron Ring Accelerator (HERA) analysis by reducing the systematic uncertainties for the Trigger efficiency, Selection efficiency, Background, Luminosity and PDF for the LHeC, and even more for the FCC-eh.

The calculated bounds at 95% C.L. for the aTGC $\Delta\kappa_\gamma$ and λ_γ are shown in Table 3. We have considered only one of the anomalous couplings to be non zero at any given time, while the other anomalous coupling is taken to zero. The bounds are computed and displayed separately for $\sqrt{s} = 1.30, 1.98, 7.07, 10$ TeV, $\mathcal{L} = 10, 30, 50, 70, 100, 300, 500, 700, 1000$ fb^{-1} and $\delta_{sys} = 0\%, 1\%, 5\%, 10\%$. As shown, our limits worsen as the systematic uncertainty value increases. The limits on $\Delta\kappa_\gamma$ do not change much, however, if the center-of-mass energy increases.

The $\sqrt{s} = 10$ TeV and $\mathcal{L} = 1000$ fb^{-1} selection has significantly better sensitivity on the aTGC $\Delta\kappa_\gamma$ and λ_γ:

$$\begin{aligned} \Delta\kappa_\gamma &= |0.00069|, \quad 95\%\ \text{C.L.}, \\ \lambda_\gamma &= [-0.0099, 0.0054], \quad 95\%\ \text{C.L.} \end{aligned} \tag{33}$$

Our bounds on anomalous $\Delta\kappa_\gamma$ and λ_γ couplings compare favorably with those reported by the ATLAS [4], CMS [5], CDF [6], D0 [7], ALEP, DELPHI, L3, OPAL [8] and TESLA [9] experiments (see Table 1). In addition, our bounds on $\Delta\kappa_\gamma$ and λ_γ are competitive with the phenomenological limits obtained using the assumed parameters of the LHC [10], the LHeC [11], the ILC [13], the CEPC [12] and the CLIC [14] as well as those of Refs. [15–32].

At the LHeC, sensitivities of $\mathcal{O}(10^{-3})$ can be reached with integrated luminosities of 10, 50 and 100 fb^{-1}. This is illustrated in Figs. 5 and 6 where we show the combined limits on $\Delta\kappa_\gamma$ and λ_γ that can be reached in $e^-p \to e^-\gamma^* p \to e^- W^- q' X$. The sensitivity bounds which can be obtained at the LHeC depend significantly on the center-of-mass and the luminosity.

Figs. 7–8 show the 95% C.L. limits expected from $e^- W^- q' X$ production on non-standard $W^+W^-\gamma$ couplings. In these figures, we presented combined contour limits in the $\Delta\kappa_\gamma - \lambda_\gamma$ plane at the FCC-he with 100, 500 and 1000 fb^{-1}, and $\sqrt{s} = 7.07, 10$ TeV in the HISZ scenario. All of these contour limits are consistent with the corresponding bounds given in Table 3.

4. Conclusions

We have studied and derived possible bounds on the aTGC $\Delta\kappa_\gamma$ and λ_γ with the $e^-p \to e^-\gamma^* p \to e^- W^- q' X$ reaction, where

Table 3
The expected 95% C.L. bounds for the anomalous couplings $\Delta\kappa_\gamma$ and λ_γ through the process $e^-p \to e^-\gamma^* p \to e^- W^- q' X$ for $\sqrt{s} = 1.30, 1.98, 7.07, 10$ TeV and $\mathcal{L} = 10, 30, 50, 70, 100, 300, 500, 700, 1000$ fb^{-1} at the LHeC and the FCC-he. The bounds for each parameter are calculated while fixing the other parameters to zero.

$\delta_{sys} = 0\%$						
Parameter	$\mathcal{L}$ (fb^{-1})	$\sqrt{s} = 1.30$ TeV	$\sqrt{s} = 1.98$ TeV	$\mathcal{L}$ (fb^{-1})	$\sqrt{s} = 7.07$ TeV	$\sqrt{s} = 10$ TeV
$\Delta\kappa_\gamma$	10	[-0.0290, 0.0283]	[-0.0195, 0.0191]	100	[-0.0027, 0.0027]	[-0.0021, 0.0021]
	30	[-0.0166, 0.0164]	[-0.0112, 0.0111]	300	[-0.0015, 0.0015]	[-0.0012, 0.0012]
	50	[-0.0128, 0.0127]	[-0.0087, 0.0086]	500	[-0.0012, 0.0012]	[-0.0009, 0.0009]
	70	[-0.0108, 0.0107]	[-0.0973, 0.0072]	700	[-0.0010, 0.0010]	[-0.0008, 0.0008]
	100	[-0.0091, 0.0090]	[-0.0061, 0.0061]	1000	[-0.0008, 0.0008]	[-0.0006, 0.0006]
λ_γ	10	[-0.1783, 0.1280]	[-0.1122, 0.0822]	100	[-0.0217, 0.0153]	[-0.0154, 0.0110]
	30	[-0.1427, 0.0923]	[-0.0895, 0.0595]	300	[-0.0174, 0.0110]	[-0.0124, 0.0079]
	50	[-0.1293, 0.0789]	[-0.0810, 0.0509]	500	[-0.0158, 0.0094]	[-0.0112, 0.0068]
	70	[-0.1214, 0.0710]	[-0.0759, 0.0459]	700	[-0.0148, 0.0084]	[-0.0105, 0.0061]
	100	[-0.1137, 0.0634]	[-0.0710, 0.0410]	1000	[-0.0139, 0.0075]	[-0.0099, 0.0054]
$\delta_{sys} = 1\%$						
$\Delta\kappa_\gamma$	100	[-0.0244, 0.0244]	[-0.0233, 0.0228]	1000	[-0.0219, 0.0214]	[-0.0218, 0.0213]
λ_γ	100	[-0.1662, 0.1159]	[-0.1209, 0.0908]	1000	[-0.0545, 0.0481]	[-0.0435, 0.0391]
$\delta_{sys} = 5\%$						
$\Delta\kappa_\gamma$	100	[-0.1186, 0.1076]	[-0.1176, 0.1061]	1000	[-0.1152, 0.1025]	[-0.1142, 0.1019]
λ_γ	100	[-0.3256, 0.2753]	[-0.2458, 0.2158]	1000	[-0.1177, 0.1113]	[-0.0944, 0.0900]
$\delta_{sys} = 10\%$						
$\Delta\kappa_\gamma$	100	[-0.2519, 0.2063]	[-0.2512, 0.2034]	1000	[-0.2495, 0.1957]	[0.2482, 0.1943]
λ_γ	100	[-0.4488, 0.3985]	[-0.3409, 0.3109]	1000	[-0.1651, 0.1587]	[-0.1326, 0.1282]

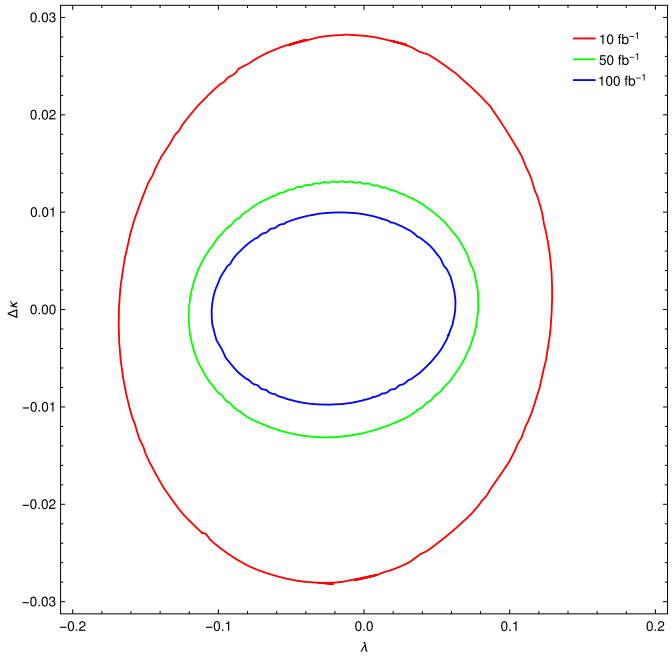

Fig. 5. Two-dimensional limits on the aTGC parameters for the combinations $\lambda_\gamma - \Delta\kappa_\gamma$ through the process $e^-p \to e^-\gamma^* p \to e^- W^- q' X$ for $\sqrt{s} = 1.30$ TeV at the LHeC. Contours for the expected 95% C.L. are shown in red, green and blue with $\mathcal{L} = 10, 50, 100$ fb^{-1}, respectively.

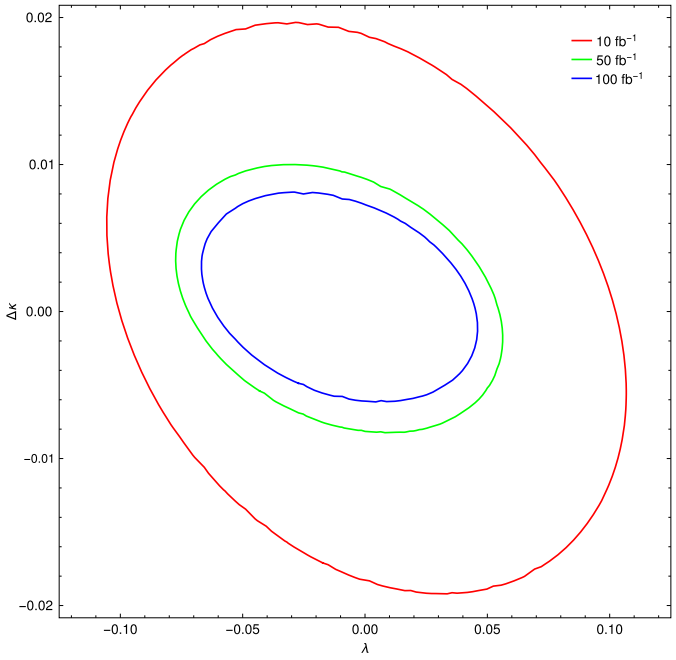

Fig. 6. The same as in Fig. 5, but for $\sqrt{s} = 1.98$ TeV and $\mathcal{L} = 10, 50, 100$ fb^{-1}, respectively.

γ^* is the quasi-real photon in the WWA, together with the total cross-section using $\mathcal{L} = 10 - 1000$ fb^{-1} of e^-p collisions, $\sqrt{s} = 1.30, 1.98, 7.07, 10$ TeV at the LHeC and the FCC-he, and $\delta_{sys} = 0\%, 1\%, 5\%, 10\%$.

The bounds obtained from our analysis on the $\Delta\kappa_\gamma$ and λ_γ parameters are comparable to the previous most stringent limits from other single-boson and diboson analyses. Furthermore, our results indicate (see Figs. 3–8 and Tables 2-3) that the $e^-p \to e^-\gamma^* p \to e^- W^- q' X$ process is potentially suitable to probe the non-standard $W^+W^-\gamma$ couplings at the LHeC and the FCC-he with cleaner environments than those for the case of hadron colliders.

As this topic is worthwhile yet underexplored, theoretical and phenomenological interest is of great importance in order to motivate experimental collaborations to measure this very intriguing sector of QED. A prominent advantage of the $e^-p \to e^-\gamma^* p \to e^- W^- q' X$ process is that it isolates anomalous $W^+W^-\gamma$ couplings, thus allowing the study of $W^+W^-\gamma$ couplings independently from W^+W^-Z and $W^+W^-\gamma\gamma$.

Declaration of competing interest

The authors declare that they have no known competing financial interests or personal relationships that could have appeared to influence the work reported in this paper.

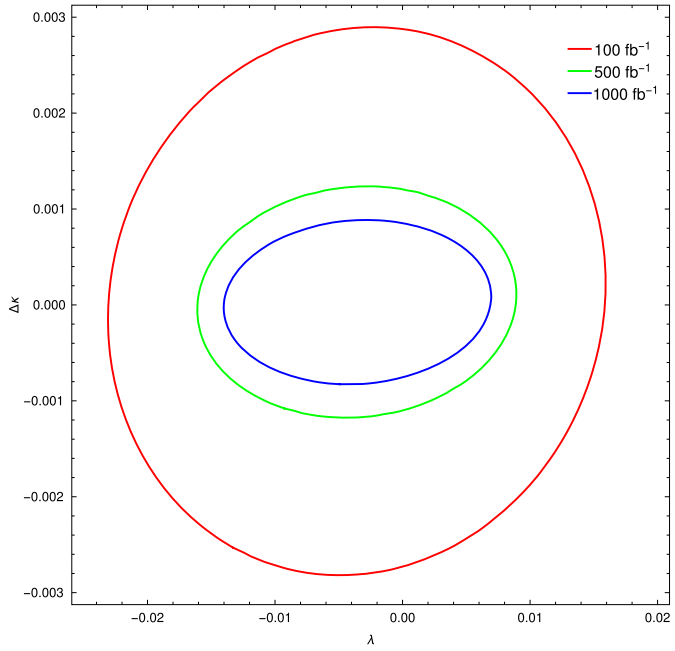

Fig. 7. Two-dimensional limits on the aTGC parameters for the combinations $\lambda_\gamma - \Delta\kappa_\gamma$ through the process $e^- p \to e^- \gamma^* p \to e^- W^- q' X$ for $\sqrt{s} = 7.07$ TeV at the FCC-he. Contours for the expected 95% C.L. are shown in red, green and blue with $\mathcal{L} = 100, 500, 1000$ fb^{-1}, respectively.

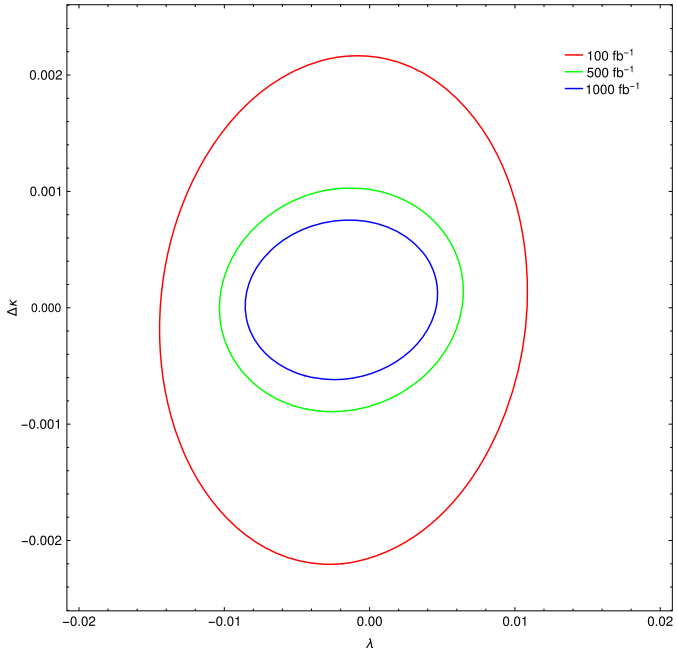

Fig. 8. The same as in Fig. 7, but for $\sqrt{s} = 10$ TeV and $\mathcal{L} = 100, 500, 1000$ fb^{-1}, respectively.

Acknowledgements

A.G.R. and M.A.H.R. thank SNI and PROFEXCE (México).

References

[1] S.L. Glashow, Nucl. Phys. 22 (1961) 579.
[2] A. Salam, J.C. Ward, Phys. Lett. 13 (1964) 168.
[3] S. Weinberg, Phys. Rev. Lett. 19 (1967) 1264.
[4] M. Aaboud, et al., ATLAS Collaboration, arXiv:1706.01702 [hep-ex].
[5] A.M. Sirunyan, et al., CMS Collaboration, Phys. Lett. B 772 (2017) 21, arXiv:1703.06095 [hep-ex].
[6] T. Aaltonen, et al., CDF Collaboration, Phys. Rev. Lett. 102 (2009) 242001.
[7] V.M. Abazov, et al., D0 Collaboration, Phys. Lett. B 718 (2012) 451, arXiv:1208.5458 [hep-ex].
[8] S. Schael, et al., ALEPH, DELPHI, L3, OPAL Collaborations and LEP Electroweak Collaborations, Phys. Rep. 532 (2013) 119, arXiv:1302.3415 [hep-ex].
[9] R.-D. Heuer, D. Miller, F. Richard, P.M. Zerwas (Eds.), TESLA Technical Design Report Part III: Physics at an e^+e^- Linear Collider, DESY, Hamburg, 2001, arXiv:hep-ph/0106315.
[10] Seyed Mohsen Etesami, Sara Khatibi, Mojtaba Mohammadi Najafabadi, Eur. Phys. J. C 76 (2016) 533.
[11] Ruibo Li, Xiao-Min Shen, Kai Wang, Tao Xu, Liangliang Zhang, Guohuai Zhu, Phys. Rev. D 97 (2018) 075043.
[12] Ligong Bian, Jing Shu, Yongchao Zhang, J. High Energy Phys. 1509 (2015) 206.
[13] H. Baer, T. Barklow, K. Fujii, Y. Gao, A. Hoang, S. Kanemura, J. List, H.E. Logan, et al., arXiv:1306.6352 [hep-ph].
[14] A.A. Billur, M. Köksal, A. Gutiérrez-Rodríguez, M.A. Hernández-Ruíz, arXiv:1909.10299 [hep-ph].
[15] A. Gutiérrez-Rodríguez, M. Köksal, A.A. Billur, M.A. Hernández-Ruíz, arXiv:1910.02307 [hep-ph].
[16] U. Baur, D. Zeppenfeld, Phys. Lett. B 201 (1988) 383.
[17] K. Hagiwara, R.D. Peccei, D. Zeppenfeld, K. Hikasa, Nucl. Phys. B 282 (1987) 253.
[18] K. Hagiwara, S. Ishihara, R. Szalapski, D. Zeppenfeld, Phys. Lett. B 283 (1992) 353.
[19] M. Diehl, O. Nachtmann, Z. Phys. C 62 (1994) 397.
[20] I. Sahin, A.A. Billur, Phys. Rev. D 83 (2011) 035011.
[21] I.T. Cakir, O. Cakir, A. Senol, A.T. Tasci, Acta Phys. Pol. B 45 (2014) 1947.
[22] V. Ari, A.A. Billur, S.C. Inan, M. Köksal, Nucl. Phys. B 906 (2016) 211.
[23] S. Atag, I.T. Cakir, Phys. Rev. D 63 (2001) 033004.
[24] S. Atag, I. Sahin, Phys. Rev. D 64 (2001) 095002.
[25] B. Sahin, Phys. Scr. 79 (2009) 065101.
[26] J. Papavassiliou, K. Philippides, Phys. Rev. D 60 (1999) 113007.
[27] D. Choudhury, J. Kalinowski, A. Kulesza, Phys. Lett. B 457 (1999) 193.
[28] E. Chapon, C. Royon, O. Kepka, Phys. Rev. D 81 (2010) 074003.
[29] John Ellis, Shao-Feng Ge, Hong-Jian He, Rui-Qing Xiao, arXiv:1902.06631 [hep-ph].
[30] Disha Bhatia, Ushoshi Maitra, Sreerup Raychaudhuri, Phys. Rev. D 99 (2019) 095017.
[31] B. Sahin, Mod. Phys. Lett. A 32 (2017) 1750205.
[32] Satendra Kumar, Poulose Poulose, Int. J. Mod. Phys. A 30 (2015) 1550215.
[33] V.M. Budnev, I.F. Ginzburg, G.V. Meledin, V.G. Serbo, Phys. Rep. 15 (1975) 181.
[34] G. Baur, et al., Phys. Rep. 364 (2002) 359.
[35] K. Piotrzkowski, Phys. Rev. D 63 (2001) 071502.
[36] J.L.A. Fernandez, et al., LHeC Study Group, J. Phys. G 39 (2012) 075001.
[37] J.L.A. Fernandez, et al., LHeC Study Group, arXiv:1211.5102.
[38] Oliver Brüning, John Jowett, Max Klein, Dario Pellegrini, Daniel Schulte, Frank Zimmermann, EDMS 17979910 FCC-ACC-RPT-0012, V1.0, https://fcc.web.cern.ch/Documents/FCCheBaselineParameters.pdf, 6 April 2017.
[39] J.L.A. Fernandez, et al., arXiv:1211.4831.
[40] Huan-Yu Bi, Ren-You Zhang, Xing-Gang Wu, Wen-Gan Ma, Xiao-Zhou Li, Samuel Owusu, Phys. Rev. D 95 (2017) 074020.
[41] Y.C. Acar, A.N. Akay, S. Beser, H. Karadeniz, U. Kaya, B.B. Oner, S. Sultansoy, Nucl. Instrum. Methods Phys. Res. 871 (2017) 47.
[42] K. Hagiwara, S. Ishihara, R. Szalapski, D. Zeppenfeld, Phys. Rev. D 48 (1993) 2182.
[43] J. Baglio, S. Dawson, I.M. Lewis, Phys. Rev. D 99 (2019) 035029.
[44] K.J.F. Gaemers, G.J. Gournaris, Z. Phys. C 1 (1979) 259.
[45] A. De Rujula, M.B. Gavela, P. Hernandez, E. Masso, Nucl. Phys. B 384 (1992) 3.
[46] I.F. Ginzburg, arXiv:1508.06581 [hep-ph].
[47] I.F. Ginzburg, G.L. Kotkin, S.L. Panfil, V.G. Serbo, V.I. Telnov, Nucl. Instrum. Methods A 219 (1984) 5.
[48] S.J. Brodsky, T. Kinoshita, H. Terazawa, Phys. Rev. D 4 (1971) 1532.
[49] H. Terazawa, Rev. Mod. Phys. 45 (1973) 615.
[50] J.M. Yang, Ann. Phys. 316 (2005) 529.
[51] A. Abulencia, et al., CDF Collaboration, Phys. Rev. Lett. 98 (2007) 112001.
[52] T. Aaltonen, et al., CDF Collaboration, Phys. Rev. Lett. 102 (2009) 222002.
[53] T. Aaltonen, et al., CDF Collaboration, Phys. Rev. Lett. 102 (2009) 242001.
[54] S. Chatrchyan, et al., CMS Collaboration, J. High Energy Phys. 1201 (2012) 052.
[55] S. Chatrchyan, et al., CMS Collaboration, J. High Energy Phys. 1211 (2012) 080.
[56] V.M. Abazov, et al., D0 Collaboration, Phys. Rev. D 88 (2013) 012005.
[57] S. Chatrchyan, et al., CMS Collaboration, J. High Energy Phys. 07 (2013) 116.
[58] S.C. Inan, Phys. Rev. D 81 (2010) 115002.
[59] S.C. Inan, Nucl. Phys. B 897 (2015) 289.
[60] S.C. Inan, Int. J. Mod. Phys. A 26 (2011) 3605.
[61] I. Sahin, S.C. Inan, J. High Energy Phys. 0909 (2009) 069.
[62] S. Atag, S.C. Inan, I. Sahin, J. High Energy Phys. 1009 (2010) 042.
[63] I. Sahin, B. Sahin, Phys. Rev. D 86 (2012) 115001.
[64] B. Sahin, A.A. Billur, Phys. Rev. D 86 (2012) 074026.
[65] A. Senol, Int. J. Mod. Phys. A 29 (2014) 1450148.
[66] A. Senol, Phys. Rev. D 87 (2013) 073003.

[67] S. Fichet, G. von Gersdorff, B. Lenzi, C. Royon, M. Saimpert, J. High Energy Phys. 1502 (2015) 165.
[68] H. Sun, Phys. Rev. D 90 (2014) 035018.
[69] H. Sun, Nucl. Phys. B 886 (2014) 691.
[70] H. Sun, Y.J. Zhou, H.S. Hou, J. High Energy Phys. 1502 (2015) 064.
[71] A. Senol, M. Köksal, J. High Energy Phys. 1503 (2015) 139.
[72] A. Belyaev, N.D. Christensen, A. Pukhov, Comput. Phys. Commun. 184 (2013) 1729.
[73] J. Pumplin, D.R. Stump, J. Huston, H.L. Lai, P. Nadolsky, W.K. Tung, J. High Energy Phys. 07 (2002) 012.
[74] A.A. Billur, et al., arXiv:1811.10462 [hep-ph].
[75] M.A. Hernández-Ruíz, et al., Nucl. Phys. B 941 (2019) 646.
[76] M. Köksal, et al., Int. J. Mod. Phys. A 34 (2019) 1950076.
[77] A. Gutiérrez-Rodríguez, et al., arXiv:1903.04135 [hep-ph].
[78] M. Köksal, et al., arXiv:1905.02564 [hep-ph].
[79] Sukanta Dutta, et al., Eur. Phys. J. C 75 (2015) 577.
[80] Néstor Armesto, et al., arXiv:1901.09076 [hep-ph].